Lab on a Chip

3-D Swimming Micro Drone Powered by Acoustic Bubbles

Journal:	*Lab on a Chip*
Manuscript ID	LC-ART-09-2020-000976.R1
Article Type:	Paper
Date Submitted by the Author:	24-Nov-2020
Complete List of Authors:	Liu, Fang-Wei; University of Pittsburgh, Mechanical Engineering Cho, Sung Kwon; University of Pittsburgh, Mechanical Engineering

Lab on a Chip

PAPER

3-D Swimming Micro Drone Powered by Acoustic Bubbles†

Fang-Wei Liu[a] and Sung Kwon Cho [*b]

Received 00th January 20xx,
Accepted 00th January 20xx

DOI: 10.1039/x0xx00000x

Mobile microrobots that maneuver in liquid environments and navigate inside human body draw great interest due to their possibility for medical uses serving as an *in vivo* cargo. For this system, the effective self-propelling method, which should be powered wirelessly and controllable in 3-D space, is of paramount importance. This article describes a bubble-powered swimming micro drone that can navigate in 3-D space in a controlled manner. To enable 3-D propulsion with steering capability, air bubbles of three lengths are trapped in microtubes that are embedded and three-dimensionally aligned inside the drone body using a two-photon polymerization. These bubbles can generate on-demand 3-D propulsion through microstreaming when they are selectively excited at their individual resonance frequencies that depend on the bubble sizes. In order to equip with highly stable maneuverability, a non-uniform mass distribution of the drone body is carefully designed to spontaneously restore the drone to the upright position from disturbances. A mathematical model of the restoration mechanism is developed to predict the restoration behavior showing a good agreement with the experimental data. The present swimming micro drone potentially lends itself to a robust 3-D maneuverable microscale mobile cargo navigating inside human body for *in vitro* and *in vivo* biomedical applications.

Introduction

Underwater, untethered, mobile swimming robots at microscale have been investigated by many groups due to their potential in serving as a navigating cargo for noninvasive and remote biomedical applications including drug delivery, biosensing, and microsurgery.[1-7] In order to realize an *in vivo* navigating micro robot, two major issues among many should be addressed: development of (1) efficient self-propulsion at microscale and (2) maneuverability in 3-D space, that is, control of propulsion direction as well as strength. As well known, the swimming environment and dynamics are characterized by the Reynolds number ($Re = UL/\nu$, where U is the characteristic speed, L the characteristic size and ν the kinematic viscosity of swimming medium) being interpreted as the ratio of inertia to viscous forces. Since micro drones are in micro scale and moving at low speed, propulsion principles should be effective for low Reynolds number environments where the viscous friction is dominant over inertia. Learning from natural creatures (e.g., bacteria) with cilia or flagella, successful thrusts in such environments generally require asymmetric reciprocating strokes in actuators.[8, 9] When the forward stroke is exactly symmetric to the backward stroke, net propulsion would not be generated in the low *Re* condition.

Currently existing micro propelling engines include using electrical or magnetic fields to drive actuators made of ferromagnetic or paramagnetic materials,[10-15] harnessing contracting cells, flagellated microorganisms, or bacteria as biohybrid swimmers,[16-21] utilizing physical or chemical gradients,[22, 23] catalytic reactions,[24-29] or acoustic excitation,[30] etc. Although some of them showed promising, they have their own drawbacks. To name a few, the biohybrids driven by microorganisms or cells have difficulty in controlling the direction and magnitude of propulsion. The methods via chemical fuels, gradients, and converting energy from light or heat are concerned with their biosafety and accessibility in live organisms. The methods using magnetic or electric fields require bulky and costly equipment to generate strong fields to penetrate into and cover the entire space of navigation.

Acoustic powering that employs resonant oscillation of gaseous bubbles is advantageous for micro propulsion due to the ease of actuation with compact and cost-effective equipment, long sustainability, relatively deep penetration into tissues, and nontoxicity to organisms. The non-zero time-averaged flow induced by an acoustically oscillating bubble, so called microstreaming, has been used to generate propulsion at microscale. One of the effective configurations to generate microstreaming is to oscillate a gaseous bubble trapped in a one-end open microtube (Fig. 1a).[31] The gas-liquid interface near the opening of the tube moves back and forth at the *high* frequency (~kHz or higher) of the acoustic excitation and

[a] Department of Mechanical Engineering and Materials Science, University of Pittsburgh, Pittsburgh, PA 15261, USA, E-Mail: FAL29@pitt.edu
[b] Department of Mechanical Engineering and Materials Science, University of Pittsburgh, Pittsburgh, PA 15261, USA, E-Mail: skcho@pitt.edu
†Electronic Supplementary Information (ESI) available: 13 movie clips are provided to enhance the understanding. See DOI: 10.1039/x0xx00000x

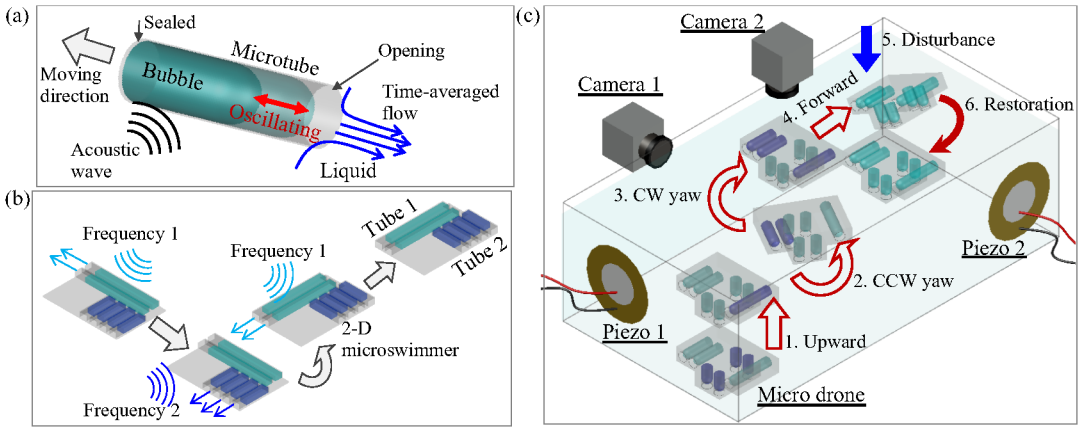

Fig. 1 (a) The non-zero time-averaged microstreaming flow generated by the acoustically oscillating gaseous bubble propels the microtube submerged in liquid environment (b) The 2-D microswimmer steers on a solid surface by two groups of microbubbles with different lengths: long bubble (light blue) and short bubble (dark blue). Each of the groups are selected and excited when the acoustic frequency matches its resonance frequency that highly depends on the bubble length. (c) The schematic and testing setup of 3-D micro swimming drone powered by three different types of microbubbles, which selectively generate propulsion forces in three directions. The bubbles trapped in the tubes can be resonantly oscillated by an external acoustic wave via the piezo actuators. The resonated bubbles (highlighted in dark blue) are generating propulsion. Note that the frequency of the acoustic wave determines which bubbles are activated. The micro drone has the capability of restoration in its orientation by carefully design the mass distribution.

generates a non-zero time-averaged net flow, microstreaming flow. Here, the Reynolds number based on the high-frequency oscillating speed is not low anymore unlike the low-frequency swimming strokes in bacteria. This means that the inertia effects play a role in generating the non-zero averaged flow that in turn acts as a reaction force on the tube. This reaction force eventually propels the tube in the opposite to the microstreaming flow direction.

Using this concept, micro swimming along the 1-D path was demonstrated.[32, 33] Moreover, the cylindrical bubble trapped in the tube has its own resonance frequency at which the generated propulsion force becomes maximum.[34] The resonance frequency critically depends on the length of the bubble for a given system. This implies that the frequency becomes a key control parameter for which bubbles are selected to turn on and off out of a group of bubbles with different lengths.[35, 36] Capitalizing these characteristics, the microswimmers with 2-D steering have been developed. The 2-D steering was achieved by embedding and orthogonally aligning two groups of microtubes differentiated by the bubble length (Fig. 1b).[35, 37] Each of them could be selectively resonated and energized by activating at its resonance frequency while the other group is suppressed in oscillation.

However, all these propelling and steering motions were limited to the 2-D solid plane. Recently, there have been attempts to generate micro swimming in a 3-D space using microstreaming. Louf *et al.* used combined actuation forces: (1) microstreaming to repel a micro swimmer made of a half capsule shell from the solid ground and (2) acoustic radiation forces to move it laterally.[38] Another approach is to use a magnetic force to assist steering in a 3-D space. Riu *et al.* introduced a magnetic force to tilt a microswimmer partially coated with a magnetic material such that the secondary Bjerknes force becomes effective to attract the microswimmer to a solid boundary.[39] As a result, the microstreaming and secondary Bjerknes force jointly generated a unidirectional force in a 3-D space. This configuration was later simplified by introducing a fin to re-direct the microstreaming flow and adjust the orientation of the microswimmer to generate secondary Bjerknes force.[40]

This article describes a 3-D maneuverable micro drone, solely powered and directed by microstreaming, which incorporates two unique designs: (1) 3-D arrangement of microtubes (bubbles) to generate independent thrusts in 3 different directions; (2) non-uniform mass distribution in the drone body to restore the drone to the upright posture and enhance stability in control.[41] To propel the drone and reach any position in a 3-D space by microstreaming requires multiple propulsion forces: for example, upward/downward in the vertical direction and clockwise/counterclockwise in yaw. In the present design, one group of micro tubes is to generate the upward propulsion while the downward motion is driven by gravity (Fig. 1c). Two more groups of tubes generate clockwise/counterclockwise yaws. This necessity brings extremely high complexity to the structure and fabrication of swimming micro drone. This challenging issue is overcome by using a 3-D printing method. A 3-D swimming micro drone with all these 3-D aligned microtubes was made within a volume less than 1 mm^3 using a two-photon polymerization 3-D printer.

In the meantime, controlling propulsion in 3-D is also highly challenging. For swimming on a 2-D surface, the solid surface on which a microswimmer sits serves as a constraint to allow the microswimmer to stay on it all the time. For swimming in a 3-D space, however, the number of spatial variables increases, and thus the control of swimming drone becomes more difficult; any external disturbances or actuations agitate the drone in a random orientation and make subsequent actuations unpredictable. It is critically necessary for the drone to automatically restore to a pre-determined posture regardless of disturbances or prior actuations. This function is achieved by re-

distributing mass in the drone body. Mismatching between the centers of mass and buoyancy always generates a restoring torque to bring the drone to the upright posture. These two unique designs facilitate highly maneuverable swimming in 3-D space, making the present swimming micro drone much closer to practical applications.

Results

First and second generation of micro drones

In order to reach any place in 3-D space, the first requisite is to generate independent thrusts in three directions. The 1st generation design of drone has three groups of microtubes assigned for upward (270 μm long) and lateral (560 and 1300 μm long) thrusts, respectively (Fig. 2a). Note that the downward motion is produced by gravity since the overall density of the drone is higher than that of the surrounding fluid. In more detail, the 8 vertically aligned microtubes (270 μm long) have the opening facing downward to generate propulsion in the positive *z*-direction, the two 1300 μm long microtubes are placed on a *x*-*y* plane to produce a linear propulsion in the *y*-direction, and the four 560 μm microtubes are located in the center region of the drone to generate a thrust in the *x*-direction.

First, the fabricated drone is tested (Fig. 2b; Video S1, Supporting Information). Initially in the absence of acoustic excitation, the drone takes an equilibrium state where the left side of the drone is slightly lower than the right side and the openings of the 270 μm microtubes face upward (first photo in Fig. 2b). This is due to the fact that the drone has more mass in the upper part. As soon as an acoustic input is given at 13.3 kHz and 5.5 volts, the 270 μm long microtubes are activated and push the drone downward against the bottom. Eventually, the drone is swimming away in a random direction and becomes uncontrollable (second and third photos in Fig. 2b).

This experiment reveals that the gravity and buoyancy forces are significantly influential to the dynamics of the drone at the present size. Learning from this unsuccessful yet instructive result, the 2nd generation of drone has been designed to investigate the dynamics and stability associated with gravity and buoyancy (Fig. 2c). Overall, the micro drone has similar dimensions in the main body and microtubes to the first generation. The main modification is that all the microtubes are located in the top half of the drone body. As a result, the density of the drone upper part is lower than that of the lower part. In order to examine the stability of the drone, the drone initially oriented in a random orientation is released without any acoustic actuation from a position several millimeters above the bottom solid surface (Fig. 2d; Video S2, Supporting Information). As the drone falls freely down to the solid surface by gravity, it automatically rotates and finally lands on the surface in the upright posture. The redistribution of microtubes generates a righting moment (restoring torque) to recover the drone to the upright position. The more detailed mechanism on this restoration is studied in the following section.

Mechanism of rotation

The above result shows that the distribution of the microtubes and mass significantly affects the balanced position and dynamics of the drone in the present sub-millimeter size. Re-distributing the microtubes in the drone body effectively relocates the center of mass. The key idea to generate a righting moment (restoring torque) is to have the center of gravity (CG) mismatched with the center of buoyancy (CB): the CG is below the CB by δ (Fig. 3a). [42, 43] The microtubes filled with air bubbles are deliberately located in the upper part of the drone. As a result, the density of the drone upper part is lower than that of the lower part since the density of the gas-filled microtube is much lower than that of the solid drone body itself. Consequently, the CG is located below the CB. Note that the location of CB is determined by the outline of the drone regardless of how microtubes are located inside the drone. Whenever disturbances or acoustic actuation forces deviate the drone from the upright posture by θ or -θ (Fig. 3b and 3d), the

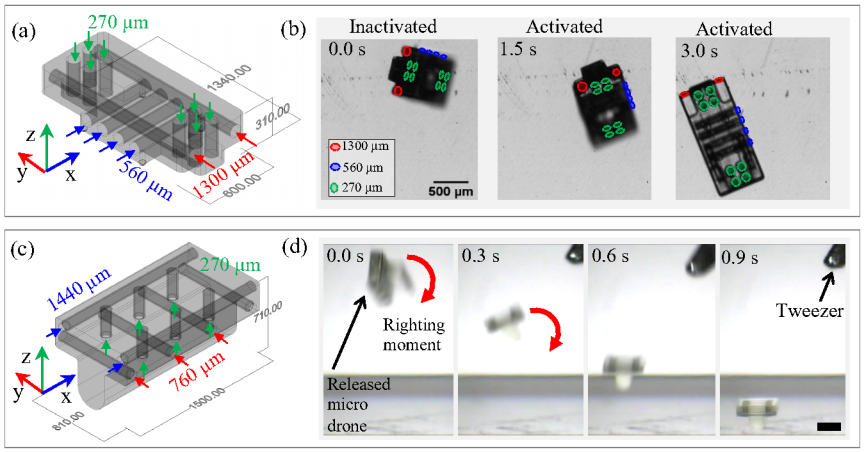

Fig. 2 (a) 1st generation of microdrone: the micro drone having microtubes distributed over the entire body and (b) its resting state and activated state by an external acoustic wave in water. The propelling motion is uncontrollable. (c) 2nd generation of microdrone: the microtubes are deliberately placed in the upper part of the body. (d) The drone automatically restores to the upright posture after being released in an initially random orientation.

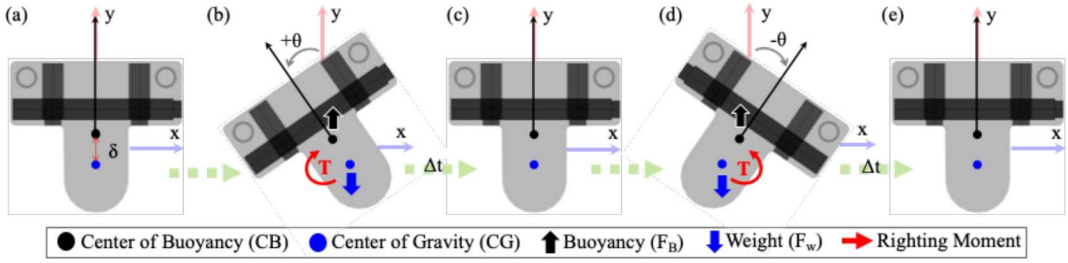

Fig. 3 Restoring mechanism: non-uniform mass distribution restores the drone to the upright position. (a) The location mismatch between CB and CG generates a restoring torque (T) when the drone is tilted. (b) and (c) show restoration from a counterclockwise tilting while (d) and (e) show restoration from a clockwise tilting.

mismatch between the CG and CB generates a restoring torque to bring the drone back to the upright position where the net torque acting on the drone is zero.

The restoration mechanism and dynamics based on this configuration can be formulated by the balance of torque on the drone about its center of gravity (CG):

$$I\frac{d^2\theta}{dt^2} + A\mu R^3\frac{d\theta}{dt} + \rho V g\delta sin\theta = 0, \quad (1)$$

where I is the moment of inertia of rolling or pitching, θ the angular displacement, A the rotating drag coefficient, μ the dynamic viscosity of the surrounding fluid, ρ is the density of the surrounding fluid, R the equivalent drone radius based on the drone volume V, g the gravity (9.8 m/s²) and δ the distance between CB and CG. The first, second and third terms in Equation (1) represent the angular momentum change, the viscous torque by friction, and the torque by the buoyancy force with the lever arm δ, respectively. The viscous torque for a sphere can be expressed as $8\pi\mu R^3\frac{d\theta}{dt}$. [44] In Equation (1), coefficient A is introduced to accommodate the geometry deviation of the drone from the sphere and later experimentally determined by curve-fitting the restoration process in the time domain. The behavior described by Equation (1) is an overdamped second order system, and can be analogous to the classic mass-spring-damper system where the time constant is obtained with an approximation of $sin\theta \approx \theta$ as:[45]

$$\tau = \frac{2I}{A\mu R^3 - \sqrt{(A\mu R^3)^2 - 4I\rho V g\delta}} \quad (2)$$

At $t = \tau$, the overdamped system reaches ~63% of its equilibrium state; at t = 4τ, ~98%. Thus, 4τ can be used as a time measure for the drone to complete its restoration process. Equation (2) provides critical information on how to design a drone, how long the acoustic signal turns on and off, and how the drone behaves dynamically.

Third generation of micro drone design

The above 2nd generation drone cannot generate any controlled yaw motion: all the 2 lateral tubes for the *x*-direction propulsion have the same length and so do all the 4 lateral tubes for the *y*-direction propulsion. In addition, in the 2nd generation design, the shortest tubes were used for the *z*-direction propulsion. However, experiments show that longer tubes generally produce stronger propulsion. Since the drone naturally sinks under no actuation, the *z*-direction needs the strongest propulsion, that is, requiring longer tubes. Based on the experiences from 1st and 2nd generations of the drone, stability analyses, and experimental trials, a few modifications from the 2nd generation are made to improve the stability and maneuverability and eventually lead to the 3rd generation design (Fig. 4.)

The more detailed features of 3rd generation micro drone are described below. The 3rd generation can steer on the x-y plane and change the elevation in the *z*-direction. Three types of microtubes are placed in different orientations and positions inside the drone body. The length and the number of each type are as follows: "Lateral 1" (890 μm long × 2), "Lateral 2" (590 μm long × 3), and "Vertical" (470 μm long × 6). In the previous studies, [33, 37] the direction of propulsion is generally opposite to the side of the microtube opening, although some exceptional cases were rarely observed in particular conditions. [46] The tube lengths of Lateral 1 and 2 are different such that they can generate clockwise as well as counterclockwise yaw motions and y-direction propulsion. Lateral 1 lying in parallel to the right rooftop plane of the microdrone generates a counterclockwise yaw; in contrast,

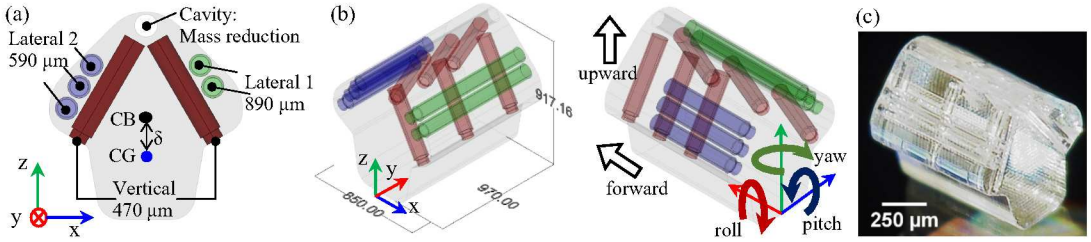

Fig. 4 3rd generation of micro drone with three groups of microtubes: (a) the front view and (b) bird's eye views. (c) The photo of fabricated 3-D micro drone taken by a 3-D digital microscope (HIROX, USA)

Lateral 2 generates a clockwise yaw. When both Lateral 1 and 2 are activated at an equal thrust, the drone propels straight forward in the positive y-direction. The overall shape (like a thick arrow) of the 3rd generation has more mass in the lower body for effective restoration. It creates a larger distance between CB and CG for restoration. In addition, the titled rooftop can more easily accommodate longer tubes to generate a stronger upward thrust overcoming the gravitational sinking. The six tilted microtubes (Vertical) parallel to the rooftop are designed to propel the microdrone upward. Here, the locations of tubes Vertical are carefully selected to compensate unbalanced mass between the sides of Lateral 1 and 2 caused by the different length of tubes Lateral 1 and 2. Note that the openings of Vertical are placed in a distance above the bottom of the drone, which facilitates stable take-off and landing from/to the ground. Otherwise, the microstreaming flow near the opening is interfered with the ground surface making propulsion more unstable.

Another unique feature in this design is to incorporate a sudden contraction near the opening of each tube. The diameter of microtubes reduces from 100 μm to 80 μm at the inner positions of 30, 50 and 70 μm from the openings for Vertical, Lateral 2 and Lateral 1, respectively. When a dried swimming drone is immersed in liquid (water or water-glycerol mixture) to trap a bubble in each tube, the water-air interface is pinned at the contraction due to re-direction of surface tension.[46] As a result, such contractions allow for uniform and consistent bubble lengths in every experiment.

When all tubes are inactive, the drone spontaneously moves downward in DI water by gravity since the overall density (1048 kg/m^3) of the drone is higher than that of the DI water (999 kg/m^3). The addition of glycerol increases the density of the liquid and thus minimizes any natural downward motion by gravity. This addition is done only where experiments need to see the pure effect of propulsion by tubes Lateral 1 and 2. Moreover, note that the viscosity of water-glycerol mixture (5:1 ratio, 1.53 x 10^{-3} Pa•s) is closer to that of the blood plasma (1.8 x 10^{-3} Pa•s) than DI water (0.9 x 10^{-3} Pa•s). In addition, a dummy cylindrical void (cavity) with both ends open in the roof corner is additionally introduced to reduce and re-distribute the mass in the upper part of the drone, as discussed in previous section. In this design, the CG is 22 μm below the CB along the gravitational line in the upright posture. The resultant density of the drone above the CB is 951 kg/m^3 while the one below is 1138 kg/m^3.

The experimental confirmation of the present drone restoring mechanism is shown in Fig. 5a and Fig. 5b (Videos S3 and S4, Supporting Information). As soon as the microdrone initially held by the tweezers in random orientations is released, the drone experiences free fall by gravity and is rolled or pitched back to the upright position. The rolling moment of inertia (I_r) is 4.25×10^{-17} kg·m^2, and the pitching moment (I_p) of inertia is 6.58×10^{-17} kg·m^2, the liquid viscosity μ ranges from 0.9 to 1.5 Pa•s, the fluid liquid density ρ ranges from 999 to 1045.4 kg/m^3 depending on the mixing ratio between DI water and glycerol, the equivalent drone radius R derived from the drone volume is 456 μm, the drone volume V is 4.9×10^{-10} m^3, and the distance between CB and CG δ is 22 μm. Using the present drone, the restoring history for rolling is measured in the time domain. As shown in Fig. 5c, the measured data in the rolling angle, the average of 21 experimental trials, are plotted along with the exact solution to Equation (1), where the dimensionless angular displacement θ/θ_o and the dimensionless time t/τ are used. Overall, they are in an excellent agreement. Using these data, coefficient A in Equation (1) is determined to be 76.6 which is about 3 times larger than 25.1 of the spherical objects, and the time constant τ of restoration is calculated to be 0.1 sec for this design. Due to the dominant viscous friction, the restoring process shows an overdamped behavior. Within 4τ or 0.4 sec, the restoring process is 98% completed, meaning that as far as the pause interval between consecutive actuations is maintained to be 0.4 sec or longer, the position of the drone is readily upright before the next actuation starts. Based on this result, a pause longer than 0.4 sec is added to the actuation signal.

3-D Maneuverability To examine the performance of the individual groups of microtubes, each type of the tube was solely activated by their resonance frequencies. The microtubes of Vertical can be excited at 11.7 kHz, and propel the microdrone upward: either taking off from the bottom of tank or moving up from a suspended position. In DI water, the

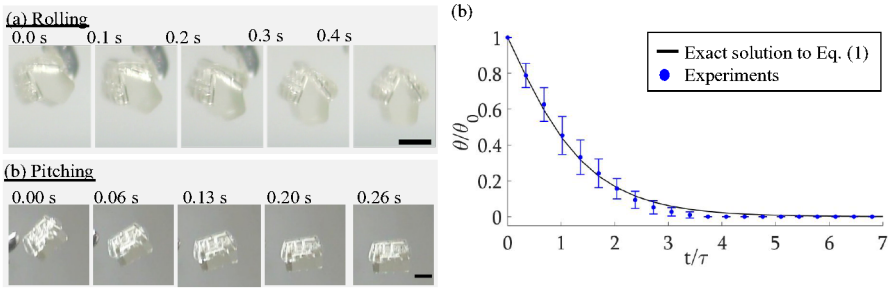

Fig. 5 Restoring results: immediately after the drone in a random rotation is released. It completely restores to the upright position within 0.4 sec by (a) rolling and (b) pitching. (c) Restoring behavior in rolling in time domain; the averaged data of 21 trials are compared with the solution to Eq. (1). Time constant τ is estimated to be about 0.1 sec. (All scale bar: 500 μm)

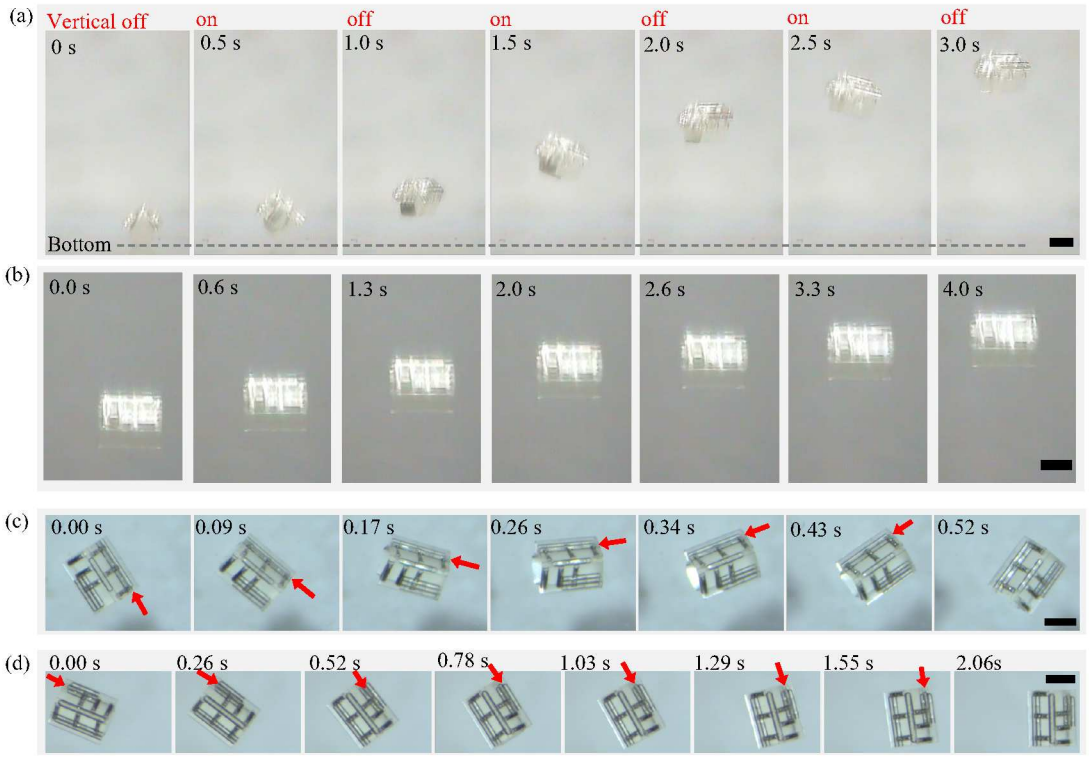

Fig. 6 Activations of individual tube types: (a) Vertical for propelling upward from the bottom, (b) Vertical for propelling upward from suspension (c) Lateral 2 for clockwise yawing, and (d) Lateral 1 for counterclockwise yawing. The red arrows show the location of the activating microtubes and its direction of propulsion. (All scale bars are 500 μm)

inactive micro drone is sitting on the bottom of the tank due to the gravity. By applying 58 V to the piezo actuator in Fig. 6a (Video S5, Supporting Information), the drone takes off and moves upward. In water-glycerol mixture, the inactive micro drone can suspend anywhere in the solution and move upward from the location by applying 24 V to the piezo-actuator (Fig. 6b, Video S6, Supporting Information) in a 3-D space. The upward speed can reach almost 4 mm/s. The efficacy of the pause signal (a pause of 0.57 sec between consecutive actuations of 0.43 sec) is clearly captured in Fig. 6a while the microdrone is propelling upward. The microdrone tilts slightly backward in the pitching angle (snapshots at 0.5, 1.5, and 2.5 sec) while the thrust is on. The above tilting is mainly attributed to the asymmetric arrangement of tubes Vertical. During the pauses after each actuation, the microdrone returns to its upright position, shown in the snapshots at 1.0, 2.0, and 3.0 sec. The activation signal for Vertical slightly affects Lateral 1 and Lateral 2, thus generating a non-negligible propulsion force by Lateral 1 and Lateral 2. Although each type of the microtube is designed to dominantly oscillate at its own resonance frequency, it can still oscillate at the off-resonance frequencies with a low magnitude and generate non-negligible propelling forces in some cases. However, this crosstalk is barely observed when Vertical is activated with the voltages below 48 V that are still high enough to elevate the drone from a suspended state (Fig. 6b).

Yawing is tested on the microdrone suspended in the water-glycerol mixture, where friction from the bottom solid surface is excluded. The microtubes of Lateral 1 are activated at 5.9 kHz, 22 V which yaws the microdrone counterclockwise (Fig. 6c; Video S7, Supporting Information), while the microtubes of Lateral 2 yaw the micro drone clockwise when excited at 7.9 kHz, 29 V (Fig. 6d; Video S8, Supporting Information). These results confirm that each type of microtubes can be independently and selectively activated by changing the activation frequency.

Consecutive and joint activations of multiple microtubes can generate a variety of propelling paths for the drone, demonstrating successful maneuverability (Fig. 7). Path 1 consists of consecutive actuations of Lateral 2 followed by Vertical conducted in DI water (Fig. 7a; Video S9 and S10, Supporting Information). First, the microdrone yaws clockwise due to the propulsion from Lateral 2 and simultaneously sinks due to the gravity. Then, the drone stops yawing as soon as Lateral 2 is deactivated. Next, as Vertical is activated, the drone moves upward against gravity. During this movement, a slight quivering of the drone can be observed. This is due to the internal noises from the instruments that occur when switching to a different frequency at relatively high voltages.

For a clearer demonstration, path 2 (Fig. 7b; Video S11, Supporting Information) is conducted in a water-glycerol mixture that has the similar density as that of the drone to eliminate the downward motion by gravity. Path 2 consists of

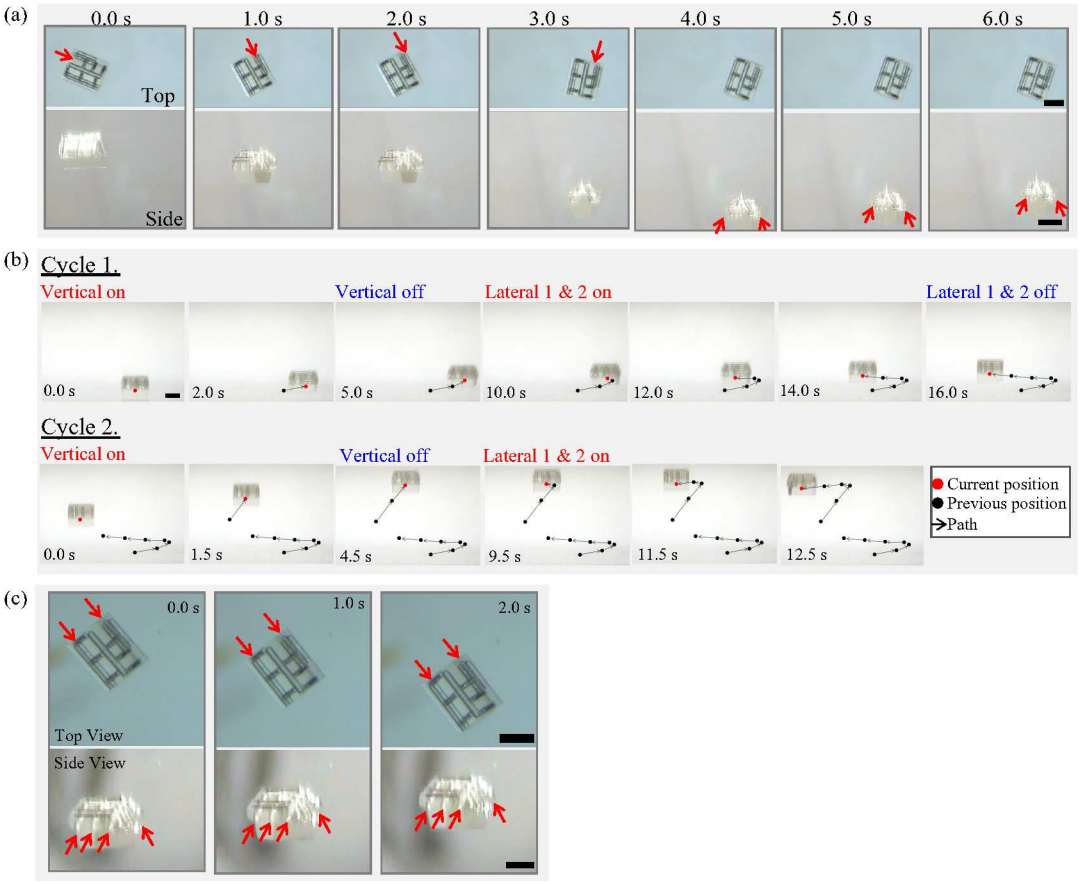

Fig. 7 (a) *Consecutive actuations* (the top and side views are recorded simultaneously). Activation of Lateral 2 resulting in turning counterclockwise but sinking due to gravity. Activating Vertical tubes elevates the drone upward. (b) *Consecutive and joint actuations.* Cycle 1.: the drone first rests on the bottom surface, then takes off by tube Vertical, and moves left by activation of tubes Lateral 1& 2. After all activations stop, the same procedure is conducted again and generates a similar motion in Cycle 2. The red dots indicate the center of drone; the black dots indicate the previous positions; the black arrows show the overall trajectory from 0.0 sec. (c) *Simultaneous actuation* of all the tubes (the top and side views are recorded simultaneously). Simultaneous activation of all types of tubes results in moving forward straight and upward (against gravity). The red arrows point the locations of activating microtubes and resultant directions of propulsions. (All scale bars are 500 μm)

two cycles of the activation of Vertical followed by the joint activation of Lateral 1 and Lateral 2. In the first cycle, the micro drone is sitting on the bottom of the tank, is lifted up when Vertical is on, and then is moved forward (left) when both Lateral 1 and 2 are on at an equal thrust (snapshots on the first row in Fig. 7b). Note that due to inequal thrusts, acoustic streaming of the surrounding liquid or background stream, the drone drifts right while moving up. After all activations stop, the micro drone loses its propulsion and suspends in the medium. Then, the same actuation procedure is conducted in cycle 2. The micro drone moves upward and then forward (left) again from the starting position.

Path 3 is accomplished by joint activations of all types of microtubes at the same time in the water-glycerol mixture. The micro drone propels upward and forward simultaneously (Fig. 7c; Video S12 and S13, Supporting Information). Based on all the results above, the micro swimming drone has the capability to reach any place in 3-D space by moving upward, downward, and forward and yawing clockwise and counterclockwise.

Discussion

The current design of swimming micro drone can provide a solution for remotely controlled underwater micro vehicles in the size of sub-millimeter range. The 3-D printing technique can reach the resolution of 200-300 nanometers, which is believed to allow the fabrication of micro drones down to tens of microns in the overall size. In this scale, the Brownian motion of the drone is expected to be not very significant. The major challenges in the scaling down of the current swimmer include the efficacy of restoration mechanism and the lifetime of the microbubbles. The performance of the drone may be limited by the prolonged restoring time as the size becomes smaller. The approximated time constant of restoration in eq. (2) shows proportional to $1/\sqrt{V\delta}$, which can roughly scale with $1/R^2$. For example, a drone of 100 μm in size would have a restoration time of about 40 sec compared to 0.4 sec of the micro drone of ~1 mm in size. This may be impractical in some applications. In the present state, we expect that the drone performs effectively

in the range of hundred microns to millimeters in the overall size.

As the bubble size becomes smaller, the acoustic frequency should increase; higher frequency ultrasound inputs should be used. Another issue in smaller scale is the lifetime of gaseous bubble. The gas in bubble dissolves faster due to the high surface-area-to-volume ratio, resulting in a shorter lifetime. However, the lifetime of bubbles can be significantly extended using the encapsulation of bubbles using a lipid layer and/or using insoluble gas [47, 48], which is commonly applied to clinically used ultrasound imaging contrast agent microbubbles. In addition, in the present study, trapping the bubble inside the microtube delays the dissolution of air to the liquid and thus increases the lifetime. Moreover, the bottle neck design (contraction near the tube opening) can improve the bubble stability during oscillation and prevent any bubble escape out of the tube. Experiments showed that the bubbles in the tube can operate for 2 – 3 hours under intermittent actuations with no significant impact on their overall propulsion and restoration behaviors and controllability. This period would be adequate for many applications.

The propulsion strength by microbubbles depends on their length as well as the response of associated components to the acoustic excitation including the piezo-actuators, amplifier, tank, etc. In addition, the resultant oscillating amplitudes of microbubbles vary from one location to another due to the reflection and dissipation of acoustic waves during propagation. This issue may be resolved by using focused beams that are uniformly exposed only to the drone and its limited surrounding area but not the entire field.

Conclusions

This article presents a swimming micro drone navigating in a 3-D space in a controlled manner, which may serve as a cargo to deliver drugs, to sense bio-signals and to perform microsurgeries in the hard-to-reach area inside human body. The drone is propelled by microstreaming flows that are generated by acoustically oscillating cylindrical bubbles. The present drone has two unique features. One is that it can be propelled in multiple directions in a controlled manner. This is realized by using multiple bubbles (tubes) of different lengths that are three-dimensionally embedded in the drone. By switching the acoustic frequencies, only resonance-frequency matched bubbles are selectively activated and generate propulsion. As a result, the drone is propelled upward or forward, and yawed clockwise or counterclockwise in an on-command manner. The downward motion is generated by gravity. By individually or jointly using these motions, the swimming micro drone is able to reach any position in a 3-D space.

The other feature is that the careful design of mass distribution in the drone significantly enhances the stability of the drone. Otherwise, the drone easily loses its orientation by any external disturbances or actuations making it extremely difficult to properly program subsequent actuations to reach the destination. The mismatch between the centers of gravity and buoyancy due to the non-uniform mass distribution generates a restoring torque to return the drone back to the upright posture all the time. This critically facilitates determining the subsequent actuation sequences and thus following a pre-determined navigating path. In addition, the mechanism of this restoration is mathematically analyzed and evaluated with experiments, showing an excellent agreement. Utilizing these features, a variety of programmed swimming paths are experimentally achieved, demonstrating the 3-D maneuverability of the swimming micro drone.

Experimental

Fabrication of Micro Swimming Drone

The swimming micro drone was fabricated by Nanoscribe Photonic Professional system (Nanoscribe GmbH, Germany), a 3D laser printer utilizing two-photon polymerization. The laser beam cures the target photoresist (IP-S, Nanoscribe GmbH, Germany) on an ITO (indium tin oxide)-coated substrate into the designed structure in micrometer scale. The configuration type is the DiLL large scale. The laser power and scanning speed are 80 mW and 90 mm/s for the shell, 90 mW and 100 mm/s for the scaffold, respectively. Afterwards, the excessive photoresist was removed by SU8-developer (MicroChem Corp., USA) followed by a rinse with isopropanol (Sigma-Aldrich, USA). The fabricated drone was then separated and released from the substrate by a razor blade and transferred to the testing tank by tweezers to be fully immersed in the solution.

Examination of Self-Recovery in Orientation

The restoration time of the microdrone was verified in a water-glycerol mixture with 5:1 volume ratio (density = 1045.4 kg m^{-3}, viscosity = 1.5 Pa·s). The microtubes in the drone automatically trapped air inside as soon as the drone was immersed in the liquid solution. The microdrone was first suspended in the solution with its upright posture, and then a disturbance was introduced by tweezers to put the micro drone into random orientations. The restoration trace from the initial orientation to the upright position was recorded in the time domain using a camera (KP-D20AU, Hitachi, Japan).

3-D Swimming

The number and the arrangement of microtubes were determined carefully in order to achieve the desired thrusts and the balanced posture in its equilibrium state. In the 3rd generation drone (Fig. 4), to generate comparable thrusts and similar total volumes of the microbubbles between the sides of Lateral 1 and Lateral 2, Lateral 1 has 2 tubes and Lateral 2 has 3 tubes. Note that the lengths of Lateral 1 and 2 are different in order to generate yawing. 3 of 6 Vertical tubes are located in the section of Lateral 1 and the others in the section of Lateral 2. Also note that their arrangement is not symmetric with respect to the y-z plane since Lateral 2 is shorter than Lateral 1.

In order to have 0° pitching as well as 0° rolling angles while in static equilibrium, 3 Vertical tubes in the side of Lateral 2 are located at larger *x* positions than those in the section of Lateral 1.

The micro swimming drone was placed in an acrylic tank (10 × 10 × 5 cm^3) filled with either DI water or water-glycerol mixture (5:1 volume ratio) solution. Two piezoelectric diaphragms (7BB-27-4L0, Murata Electronics, resonance frequency of 4.6 kHz, Japan) were glued to the sidewalls of the tank and connected to a function generator with an amplifier. The frequency to activate each type of the microtubes was first determined by preliminary frequency-sweeping experiments. A small slab embedded with the three tubes of different lengths was fabricated using the Nanoscribe 3-D laser printer. After submerging the slab, the amplitude of oscillation of each microbubble was recorded while sweeping the frequency from 3 to 15 kHz with an increment of 0.1 kHz but maintaining the voltage amplitude (to the piezo-actuator) constant. The frequency spectrum for each bubble show multiple peaks. By cross-checking the three frequency spectra, the actuating frequency of each bubble was determined among the peak frequencies, which was not coincided with or too close to the peak frequencies in the other two spectra. This selection procedure ensures to minimize the interference or any cross talks among the three bubble actuations. The more detailed procedure is described in ref. 37. The individual activation frequencies of the 3rd generation drone are 5.9 kHz for Lateral 1, 7.9 kHz for Lateral 2, and 11.7 kHz for Vertical. These frequencies deviate from the theoretical prediction (6.9, 10, 14.5 kHz, respectively) based on the model in ref. 31. This is due to the fact that the bubble oscillation is affected by the entire system setup including the frequency responses of the tank, piezo-actuator, supporting structures, etc., as studied in the previous work.[37] The theoretical model may be valid only for the bubble submerged in the infinite liquid but does not take into account the effect of the associated components.

For the joint activation, 6.2 kHz is used to generate a forward motion as it induces similar thrusts by both Lateral 1 and Lateral 2 but keeps propulsion by Vertical negligible and requires a single channel amplification. This frequency was also determined experimentally.

Conflicts of interest

There are no conflicts to declare.

Acknowledgements

This work is supported by National Science Foundation (ECCS-1637815).

References

1. M. P. Kummer, J. J. Abbott, B. E. Kratochvil, R. Borer, A. Sengul and B. J. Nelson, *IEEE Trans. Robot.*, 2010, **26**, 1006-1017.
2. T. Mirkovic, N. S. Zacharia, G. D. Scholes and G. A. Ozin, *ACS Nano*, 2010, **4**, 1782-1789.
3. B. J. Nelson, I. K. Kaliakatsos and J. J. Abbott, *Annu. Rev. Biomed. Eng.*, 2010, **12**, 55-85.
4. J. Wu, S. Balasubramanian, D. Kagan, K. M. Manesh, S. Campuzano and J. Wang, *Nat. Commun.*, 2010, **1**, 36.
5. D. Patra, S. Sengupta, W. Duan, H. Zhang, R. Pavlick and A. Sen, *Nanoscale*, 2013, **5**, 1273-1283.
6. M. Sitti, H. Ceylan, W. Hu, J. Giltinan, M. Turan, S. Yim and E. Diller, *Proc. IEEE Inst. Electr. Electron. Eng.*, 2015, **103**, 205-224.
7. A. K. Singh and M. Sitti, *Curr. Pharm. Des.*, 2016, **22**, 1418-1428.
8. E. M. Purcell, *Am. J. Phys.*, 1977, **45**, 3-11.
9. J. Feng and S. K. Cho, *Micromachines*, 2014, **5**, 97-113.
10. G. Hwang, R. Braive, L. Couraud, A. Cavanna, O. Abdelkarim, I. Robert-Philip, A. Beveratos, I. Sagnes, S. Haliyo and S. Régnier, *Int. J. Robotics Res.*, 2011, **30**, 806-819.
11. X. Yan, Q. Zhou, J. Yu, T. Xu, Y. Deng, T. Tang, Q. Feng, L. Bian, Y. Zhang, A. Ferreira and L. Zhang, *Adv. Funct. Mater.*, 2015, **25**, 5333-5342.
12. A. Barbot, D. Decanini and G. Hwang, *Sci. Rep.*, 2016, **6**, 19041-19048.
13. A. M. Maier, C. Weig, P. Oswald, E. Frey, P. Fischer and T. Liedl, *Nano Lett.*, 2016, **16**, 906-910.
14. X. Wang, C. Hu, L. Schurz, C. D. Marco, X. Chen, S. Pané and B. J. Nelson, *ACS Nano*, 2018, **12**, 6210-6217.
15. U. K. Cheang, D. Roy, J. H. Lee and M. J. Kim, *Appl. Phys. Lett.*, 2010, **97**, 213704.
16. E. Steager, C.-B. Kim, J. Patel, S. Bith, C. Naik, L. Reber and M. J. Kim, *Appl. Phys. Lett.*, 2007, **90**, 263901.
17. E. B. Steager, M. S. Sakar, D. H. Kim, V. Kumar, G. J. Pappas and M. J. Kim, *J. Micromech. Microeng.*, 2011, **21**, 035001.
18. B. J. Williams, S. V. Anand, J. Rajagopalan and M. T. A. Saif, *Nat. Commun.*, 2014, **5**, 3081.
19. H. Kim and M. J. Kim, *IEEE T. Robot.*, 2015, **32**, 125-137.
20. M. M. Stanton, B.-W. Park, A. Miguel-López, X. Ma, M. Sitti and S. Sánchez, *Small*, 2017, **13**, 1603679.
21. B.-W. Park, J. Zhuang, O. Yasa and M. Sitti, *ACS Nano*, 2017, **11**, 8910-8923.
22. H.-R. Jiang, N. Yoshinaga and M. Sano, *Phys. Rev. Lett.*, 2010, **105**, 268302.
23. C. Maggi, F. SaglimbenI, M. Dipalo, F. D. Angelis and R. D. Leonardo, *Nat. Commun.*, 2015, **6**, 7855.
24. J. R. Howse, R. A. L. Jones, A. J. Ryan, T. Gough, T. Vafabakhsh and T. Golestanian, *Phys. Rev. Lett*, 2007, **99**, 48102- 48105.
25. S. Sundararajan, P. E. Lammert, A. W. Zudans, V. H. Crespi and A. Sen, *Nano Lett.*, 2008, **8**, 1271-1276.
26. W. Gao, K. M. Manesh, J. Hua, S. Sattayasamitsathit and J. Wang, *Small*, 2011, **7**, 2047-2051.
27. W. Gao, A. Uygun and J. Wang, *J. Am. Chem. Soc.*, 2012, **134**, 897-900.
28. W. Gao and J. Wang, *Nanoscale*, 2014, **6**, 10486-10494.
29. V. Sridhar, F. Podjaski, J. Kröger, A. Jiménez-Solano, B.-W.Park, B. V. Lotsch and M. Sitti, *PNAS*, 2020, **117**, 24748-24756.

30. M. Kaynak, A. Ozcelik, A. Nourhani, P. E. Lammert, V. H. Crespi and T. J. Huang, *Lab Chip*, 2017, **17**, 395-400.
31. R. J. Dijkink, J. P. V. d. Dennen, C. D. Ohl and A. Prosperetti, *J. Micromech. Microeng*, 2006, **16**, 1653-1659.
32. J. Feng and S. K. Cho, presented in part at the IEEE 26th International Conference on Micro Electro Mechanical Systems (MEMS), Taipei, Taiwan, 2013.
33. J. Feng, J. Yuan and S. K. Cho, *Lab Chip*, 2015, **15**, 1554-1562.
34. H. N. Oğuz and A. Prosperetti, *JASA*, 1998, **103**, 3301-3308.
35. J. Feng and S. K. Cho, presented in part at the 2014 IEEE 27th International Conference on Micro Electro Mechanical Systems (MEMS), San Francisco, CA, USA, 2014.
36. D. Ahmed, M. Lu, A. Nourhani, P. E. Lammert, Z. Stratton, H. S. Muddana, V. H. Crespi and T. J. Huang, *Sci. Rep.*, 2015, **5**, 9744-9751.
37. J. Feng, J. Yuan and S. K. Cho, *Lab Chip*, 2016, **16**, 2317-2325.
38. J. F. Louf, N. Bertin, B. Dollet, O. Stephan and P. Marmottant, *Adv. Mater. Interfaces*, 2018, **5**, 1800425.
39. L. Ren, N. Nama, J. M. McNeill, F. Soto, Z. Yan, W. Liu, W. Wang, J. Wang and T. E. Mallouk, *Sci. Adv.*, 2019, **5**, eaax3084.
40. A. Aghakhani, O. Yasa, P. Wrede and M. Sitti, *PNAS*, 2020, **117**, 3469-3477.
41. F.-W. Liu and S. K. Cho, presented in part at the IEEE 32th International Conference on Micro Electro Mechanical Systems (MEMS), Seoul, South Korea, 2019.
42. Y.-L. Wang and C.-Y. Lu, *j. Mar. Eng. Technol.*, 2012, **11**, 39-48.
43. R. Capocci, G. Dooly, E. O.́, J. Coleman, T. Newe and D.Toal, *J. Mar. Sci. Eng.* , 2017, **5**, 13.
44. H. Lamb, *Hydrodynamics*, Cambridge University Press, 6th edn., 1932.
45. A. A. Shabana, *Theory of vibration: an introduction*, Springer, Cham, 3 edn., 2019.
46. F.-W. Liu, Y. Zhan and S. K. Cho, presented in part at the IEEE 31th International Conference on Micro Electro Mechanical Systems (MEMS), Belfast, Northen Ireland, 2018.
47. S. Singhal, C. Moser and M. A. Wheatle, *Langmuir*, 1993, **9**, 2426-2429.
48. K. Ferrara, R. Pollard and M. Borden, *Annual Review of Biomedical Engineering*, 2007, **9**, 415-477.

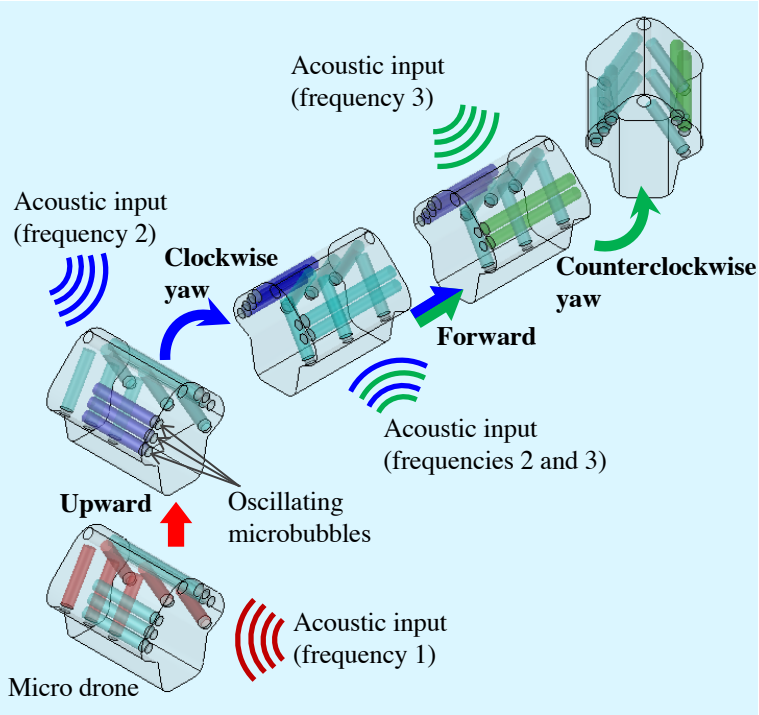

The swimming microdrone can navigate with high maneuverability in 3D space powered by remote acoustic waves.